

Macroscopic Phase-Field Model of Partial Wetting: Bubbles in a Capillary Tube

Luis Cueto-Felgueroso and Ruben Juanes

Massachusetts Institute of Technology, 77 Massachusetts Avenue, Building 48, Cambridge, Massachusetts 02139, USA

(Received 28 July 2011; published 5 April 2012)

Drops and bubbles are nonspreading, local, compactly supported features. They are also equilibrium configurations in partial wetting phenomena. Yet, current macroscopic theories of capillary-dominated flow are unable to describe these systems. We propose a framework to model multiphase flow in porous media with nonspreading equilibrium configurations. We illustrate our approach with a one-dimensional model of two-phase flow in a capillary tube. Our model allows for the presence of *compactons*: nonspreading steady-state solutions in the absence of external forces. We show that local rate dependency is not needed to explain globally rate-dependent displacement patterns, and we interpret dynamic wetting transitions as the route from equilibrium, capillary-dominated configurations, towards viscous-dominated flow. Mathematically, these transitions are possible due to nonclassical shock solutions and the role of bistability and higher-order terms in our model.

DOI: 10.1103/PhysRevLett.108.144502

PACS numbers: 47.55.N-, 47.55.dr, 47.56.+r, 68.08.Bc

Multiphase flow systems are often described by using upscaled mathematical models, aimed at capturing the relevant flow mechanisms while keeping the problem tractable in a computational or analytical sense. Upscaling procedures invoke approximations that reduce the dimensionality of the models, write equations at a scale that is much larger than the typical capillary length, or both. Examples are ubiquitous in fluid mechanics, from Lucas-Washburn laws during imbibition in nanopores [1,2] to basin-scale models of CO₂ migration in geologic carbon sequestration [3]. Assumptions of vertical flow equilibrium, or the lubrication approximation, permit reducing the dimensionality of thin film flows [4,5] and gravity currents [6], usually described by evolution equations for the height of the interface. By averaging the pore-scale processes over a representative elementary volume, multiphase flow through porous media is modeled by balance laws written in terms of fluid volume fractions, or *saturations* [7]. Necessarily, all these upscaled descriptions lead to loss of information about complex small-scale flow features. What is surprising, and disturbing, is that current theories fail to describe simple capillary phenomena, like a droplet on a flat surface or an air bubble at rest in a capillary tube [Fig. 1(a)]. The origin of the problem seems to lie in the macroscopic description of nonspreading systems associated to partial wetting.

The equilibrium shape of a water droplet deposited on a flat solid surface illustrates two regimes in wetting phenomena [8,9]. In the *complete wetting* regime, the droplet spreads over the solid surface, ultimately leaving a microscopic film attached to the solid. In the *partial wetting* regime, the droplet relaxes towards an equilibrium configuration, characterized by a *static* contact angle θ . The transition from complete to partial wetting, or from spreading to nonspreading systems, is controlled by the interfacial energies through the spreading coefficient,

$\Sigma = \gamma_{sa} - (\gamma_{sw} + \gamma)$, where γ is the surface tension between the two fluids and γ_{sa} and γ_{sw} are the surface tensions associated with solid-fluid interfaces. Spreading systems ($\Sigma \geq 0$) are relatively well understood, and diffusive scaling laws for the evolution of relevant quantities have been derived and confirmed experimentally [1,5,8,9]. Nonspreading systems ($\Sigma < 0$), however, continue to challenge our mathematical descriptions. In some cases, such as thin film flows, the difficulty arises from the description of the dynamics of the contact line [5]. In volume-fraction-based models, the problem can be stated in mathematical

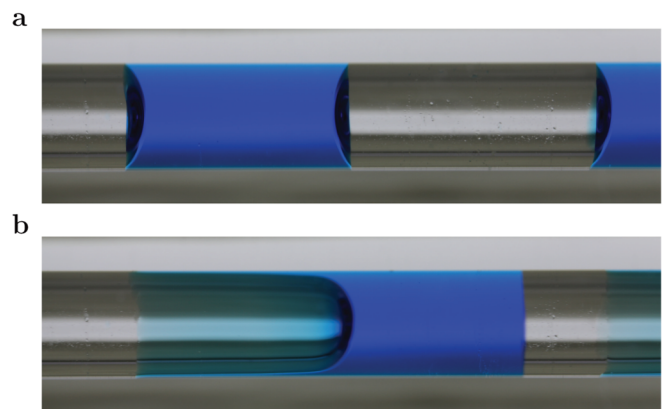


FIG. 1 (color online). Statics and dynamics of fluid slugs in a capillary tube. (a) Static configuration of an air bubble (transparent) between two slugs of water (dyed blue) in a glass capillary tube. The liquid-gas interface exhibits a well-defined contact angle, characteristic of a system with partial wetting. (b) Snapshot of an advancing liquid slug, blown by air from left to right. The leading interface advances with a contact angle that is larger than the static contact angle. At the back end of the slug, air penetrates through the center of the tube and leaves a macroscopic film of viscous fluid attached to the walls. The advancing contact angle and the film thickness are rate-dependent.

terms: how to obtain local, nonspreading, and compactly supported features—bubbles in a capillary tube—as steady-state solutions of a scalar, parabolic conservation law. Here, we address this latter challenge. We build a model of two-phase flow (e.g., air displacing water) in a capillary tube, which describes the flow dynamics through the evolution of gas and water saturations, S_g and S_w , respectively, along the tube. The saturation of a fluid is the fraction of the cross-sectional area of the tube occupied by that fluid. Our simple 1D model captures hitherto unexplored capillary phenomena by accurately reproducing the thermodynamic equilibrium of the system. One of the fundamental advances in our model is that the steady-state solutions are bubbles or fluid slugs—local, nonspreading, compactly supported features.

The transition from the capillary-dominated to the viscous-dominated regimes is another fascinating aspect of our model. Physically, multiphase systems often exhibit “dynamic” behavior, that is, flow features that are rate-dependent, like contact angles [8–11], displacement efficiencies [12–14], capillary pressures [15–17], fractional flow [18], or displacement pattern morphologies [19–21]. For instance, when air is injected at a constant rate in a tube initially filled with a viscous fluid, the invading air forms an advancing finger that leaves a macroscopic film of the viscous fluid attached to the tube walls [Fig. 1(b)] [12,13]. The thickness of the film increases monotonically with the capillary number $Ca = U\eta_w/\gamma$, where U is the velocity of the finger tip, η_w is the viscosity of the defending fluid, and γ is the surface tension between the fluids [14,22–24]. Here, we show that rate dependency of the global displacement patterns, such as the amount of fluid left behind in the classical Bretherton experiment, can be explained and modeled as the competition between capillary and viscous forces, without resorting to rate-dependent constitutive relations.

We consider incompressible, isothermal two-phase flow in a tube, driven by imposed pressure gradients and capillary forces. The evolution of fluid saturations can be expressed as conservation of mass of the fluids, $\partial_t S_\alpha + \partial_x u_\alpha = 0$ with $\alpha = g, w$, subject to the constraint $S_g + S_w \equiv 1$. We assume gradient-type volumetric fluxes $u_\alpha = -\lambda_\alpha \partial_x \Pi_\alpha$, where λ_α denotes the mobility of phase α . In the classical models, the flow potentials Π_α are identified as averaged fluid pressures [7,17]. In contrast, we follow the framework of E and Palfy-Muhoray for incompressible polymer mixtures [25,26] and split the potentials as $\Pi_\alpha = \mu_\alpha + p + \rho_\alpha g z$, where μ_α is the chemical potential derived from a phenomenological free energy functional of the two-component system, p is the pressure, which enforces the incompressibility constraint, ρ_α is the fluid density, and g is the gravitational acceleration. After algebraic manipulation, assuming for now a horizontal tube, and using gas saturations as primary variables, the model reads

$$\partial_t S_g + \partial_x (f_g u_T + \lambda_g (1 - f_g) \partial_x (\mu_w - \mu_g)) = 0, \quad (1)$$

$$\partial_x u_T = 0, \quad (2)$$

$$u_T = -[(\lambda_g + \lambda_w) \partial_x \Pi_g + \lambda_w \partial_x (\mu_w - \mu_g)]. \quad (3)$$

The fractional flow function $f_g = \lambda_g / (\lambda_g + \lambda_w)$ is a nonconvex, S -shaped function of the gas saturation that controls the viscous-dominated flow regime. Closure of the model (1)–(3) requires specifying constitutive relations for the fluid mobilities λ_α and the thermodynamic potentials μ_α . We set the gas and water mobilities as $\lambda_g = R^2 S_g / 8\eta$ and $\lambda_w = R^2 S_w^3 / 8\eta$, respectively, where R is the radius of the tube and $\eta(S_g)$ is an averaged viscosity of the mixture. For simplicity, we assume that η^{-1} is linear with the fluid saturations: $\eta^{-1} = \eta_w^{-1} + (\eta_g^{-1} - \eta_w^{-1}) S_g$.

The chemical potential difference $\mu_w - \mu_g$ plays a central role in the structure of saturation profiles at equilibrium ($u_T = 0$). In traditional models, this difference in chemical potential is understood as a monotonic function of the phase saturation—the so-called capillary pressure function [7]. While a term of such nature can describe diffusive, spreading behavior [1,7], nonspreading static structures, like a simple stationary bubble in a capillary tube, are precluded in the absence of external forces. Inspired by phase-field modeling [25–28], we derive the chemical potentials μ_α from a phenomenological free energy functional F of the system.

To construct the F functional, we follow the classical theory of phase separation of Cahn and Hilliard [27], and de Gennes’s model for incompressible polymer mixtures [25]. We approximate the specific free energy as the sum of bulk, F_0 , and interfacial, F_i , free energies. The former is solely a function of fluid saturations, while the latter includes gradient terms: $F = F_0(S_g, S_w) + F_i(S_g, S_w, \nabla S_g, \nabla S_w)$. Our basic requirements are that two stable states of the free energy correspond to the bulk fluids, $S_g = 1$ and $S_w = 1$, and that differences in chemical potential between bulk fluids are consistent with the Young-Laplace equation $[[\mu_g]] = 2\gamma \cos\theta / R$, where $[[\mu_g]] = \mu_g|_{S_g=1} - \mu_g|_{S_g=0}$. The simplest specific free energy satisfying these conditions is

$$F = -\frac{\gamma_{sw} - \gamma_{sg} - \gamma}{R} (1 - S_g)^2 (1 - S_w)^2 + \frac{\gamma_{sw} - \gamma_{sg}}{R} [(1 - S_g)^2 - (1 - S_w)^2] + \frac{\Gamma}{4} \kappa(S_g, S_w) ((\partial_x S_g)^2 + (\partial_x S_w)^2). \quad (4)$$

In the following, we consider strictly nonspreading systems, $\gamma_{sw} - \gamma_{sg} - \gamma < 0$, for which the three surface energies are linked through the static contact angle, $\gamma_{sw} - \gamma_{sg} = \gamma \cos\theta$. Note that we define the contact angle θ with respect to the “gas” phase, regardless of which phase is more dense. Based on the above free energy, the

common-tangent construction [29] yields, for arbitrary contact angles $0^\circ < \theta \leq 180^\circ$ and along $S_w = 1 - S_g$, the stable states $S_g = 0$ and $S_g = 1$. The structure of the function multiplying the square concentration gradients is essential to obtain compactons [30]. The constant Γ has units of force, and, heuristically, we take $\kappa = S_g^\alpha S_w^\beta$, with $\alpha = 2 - \frac{1}{2} \cos\theta$ and $\beta = 2 + \frac{1}{2} \cos\theta$. The strength of Γ is set to yield the correct width of the meniscus, δ , where $\delta = R|(1 - \sin\theta)/\cos\theta|$ for spherical-cap menisci (Fig. 2). Since the interfacial width emerges from a balance between the gradient energy term and the double well, $\delta^2 \sim \Gamma R/\gamma(1 - \cos\theta)$, we take $\Gamma = C_\Gamma \gamma R(1 - \cos\theta)((1 - \sin\theta)/\cos\theta)^2$, where $C_\Gamma \approx 3/2$ seems to yield the correct δ .

The chemical potentials μ_g and μ_w are the variational derivatives of the free energy with respect to the fluid saturations: $\mu_\alpha \equiv \delta F/\delta S_\alpha = \partial F/\partial S_\alpha - \partial_x(\partial F/\partial(\partial_x S_\alpha))$. Thus,

$$\begin{aligned} \mu_w - \mu_g = & -\frac{2\gamma \cos\theta}{R} \\ & -\frac{2\gamma(1 - \cos\theta)}{R} S_g(1 - S_g)(1 - 2S_g) \\ & + \Gamma \sqrt{\kappa} \partial_x(\sqrt{\kappa} \partial_x S_g), \end{aligned} \quad (5)$$

where we have used the identity $S_w = 1 - S_g$.

The model (1)–(3), together with the above definition (5), retains in part the classical structure of models of multiphase flow in porous media. The saturation equation is a conservation law with an S -shaped fractional flow and a nonlinear diffusion term. In the limit of zero dissipation, Eq. (1) is a hyperbolic equation with Lax shock solutions. Under static conditions $Ca \rightarrow 0$, classical models predict spreading, or capillary redistribution. In our model, the fourth-order term and the phase-segregating bulk potential lead to a completely different behavior. At static equilibrium, saturation profiles are nonspreading compactons, that is, regions of pure fluid phases (bubbles) separated by transition regions (menisci); see Fig. 1(a). When driven out of equilibrium, through the imposition of a pressure gradient or constant flow rate, the displacement pattern depends on Ca [Fig. 1(b)]. This behavior emerges naturally from the competition between the advective and higher-order terms.

We numerically solve the steady states of the transport equation (1) under static conditions $u_T = 0$ (Fig. 2). An important consequence of the emergence of compacton solutions is that equilibrium configurations may comprise several small bubbles rather than a single, larger one. A similar result of multiple local minima due to compactly supported solutions was recently found in a phase-field model of phase separation [30], where the authors show the critical role of a nonlinear coefficient multiplying the square-gradient term in the free energy, which vanishes at $S_g = 0$ and $S_g = 1$. In our model, the structure of this nonlinear term also determines the curvature of the

transitions (menisci) for a given static contact angle. By construction, the free energy functional [Eq. (4)] leads to pressure jumps across interfaces that are consistent with the Young-Laplace equation.

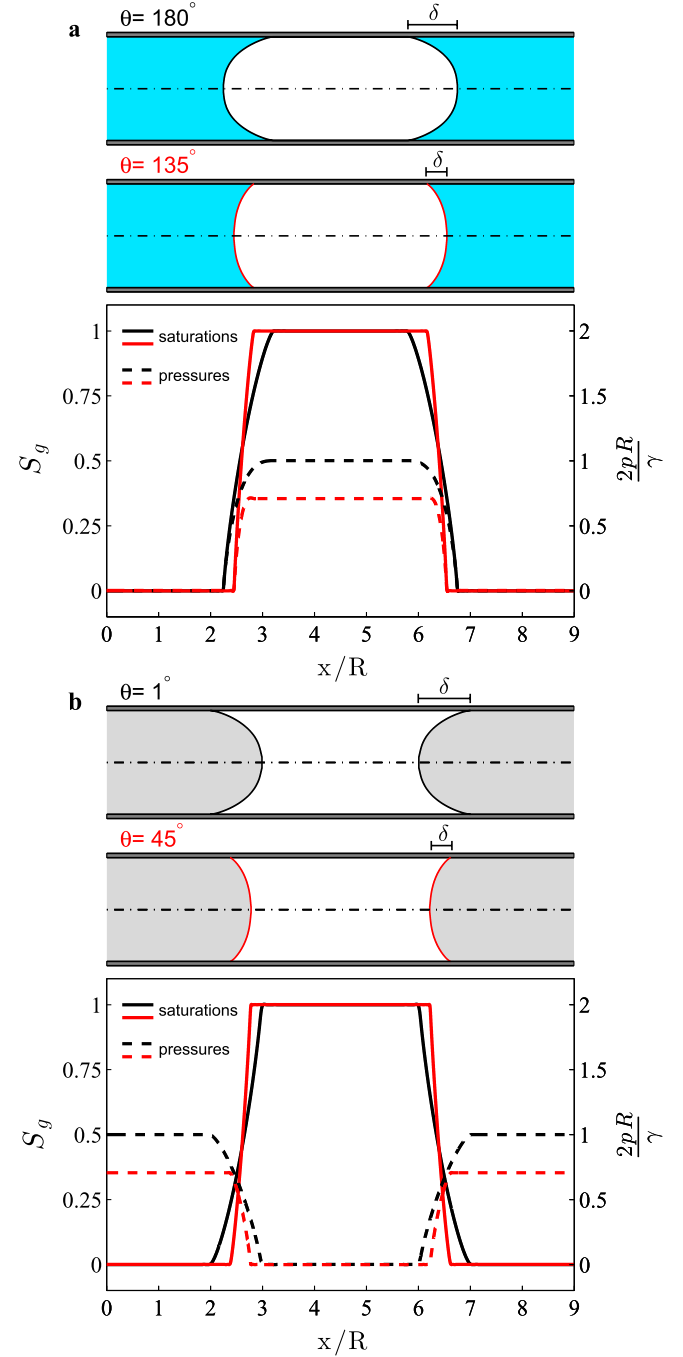


FIG. 2 (color online). (a),(b) Steady-state configurations, obtained by numerically solving the model equations (1)–(3) with $u_T = 0$, and their axisymmetric interpretation of the fluid distribution along the tube: a gas bubble surrounded by a wetting fluid such as water (a) or by a nonwetting fluid such as mercury (b). The position of the interface is determined as $h_g = \sqrt{S_g}$ for $\theta > 90^\circ$ and $h_g = \sqrt{1 - S_g}$ for $\theta < 90^\circ$. The equilibrium saturation and pressure profiles change with the static contact angle.

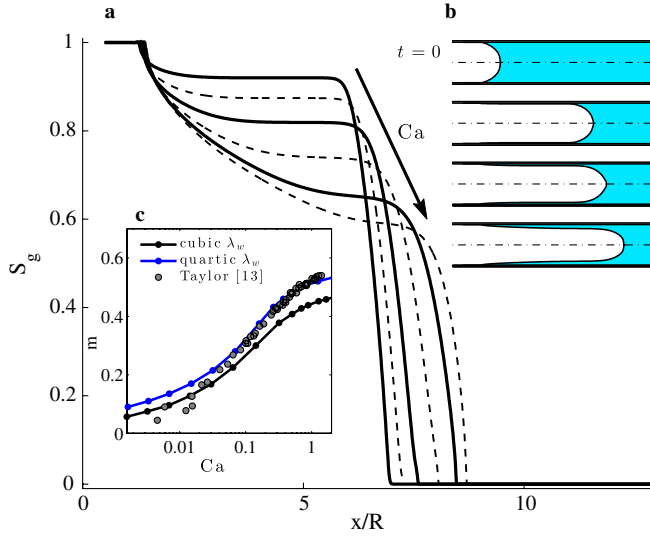


FIG. 3 (color online). Simulations of air injection at a constant rate in a tube filled with a viscous fluid, where we assume a static contact angle $\theta = 180^\circ$. (a) Gas saturation profiles for different capillary numbers. The volume of gas injected is the same in all cases. The transition from a finger that leaves a thick film for large Ca to the static case with phase separation at $Ca \rightarrow 0$ results from the relative dominance of the hyperbolic or higher-order terms, respectively. For intermediate capillary numbers, the gas saturation profiles exhibit nonclassical shocks with a plateau. (b) Distribution of fluids inside the tube, obtained from the computed saturation profiles. (c) Comparison of the mass fraction of viscous fluid left behind, m , with the experimental results of Taylor [13]. We set $m = 1 - S_g^*$, where S_g^* is the plateau gas saturation. We compare the model predictions with two functional forms of the water mobility, namely, $\lambda_w \sim S_w^3$ and $\lambda_w \sim S_w^4$.

To test the ability of our model to capture the dynamic features of air-water displacements, we simulate constant-rate air injection into a water-filled circular tube (Fig. 3). We explain the classical experimental observations

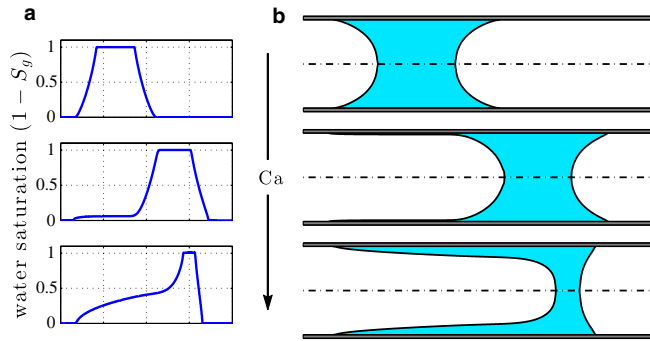


FIG. 4 (color online). Contact-line motion and dynamic contact angle in the displacement of a water slug by air. (a) Water saturation profiles for various injection rates (the top figure corresponds to the static configuration $Ca = 0$). (b) Axisymmetric interpretation of the fluid distribution inside the tube. Higher capillary numbers lead to higher dynamic contact angles, in accordance with the classical experiments of Hoffman [8,10].

[12–14], in which a film of the defending fluid is left attached to the tube walls, as a result of the competition between capillary and viscous forces. In our model, capillary terms induce phase separation and therefore a complete displacement of the resident fluid, while viscous forces, represented by the hyperbolic term in Eq. (1), tend to create a fast displacement along the center of the tube that leaves a film of the more viscous fluid behind. Our simulations honor this behavior: At small capillary numbers, the meniscus advances through contact-line motion. Mathematically, the parabolic term dominates, and therefore the behavior of the solutions resembles phase separation. For large capillary numbers, viscous forces dominate, and thick water films are left behind attached to the walls [Fig. 3(b)]. In mathematical terms, the hyperbolic term dominates, and the saturation profile resembles the classical Lax shock solution [Fig. 3(a)]. For intermediate capillary numbers, the gas saturation profiles exhibit undercompressive shocks with a plateau, induced by the structure of the bulk free energy and the presence of the fourth-order term [31].

Under dynamic conditions, which drive the system out of capillary equilibrium, the symmetry of displaced bubbles or slugs is broken as the capillary number increases. We simulate the displacement of a capillary bridge by air at a constant rate (Fig. 4). In quasistatic conditions $Ca \rightarrow 0$, the water slug is displaced almost completely, and therefore the symmetry is essentially retained: The advancing and receding contact angles are similar. Higher capillary numbers lead to steeper fronts, inducing a transition. As $Ca \rightarrow \infty$, the symmetry is lost, and films are left behind. In accordance with the classical experiments of Hoffman [8,10], the advancing contact angle increases with the flow rate. This effective dynamic behavior of the contact

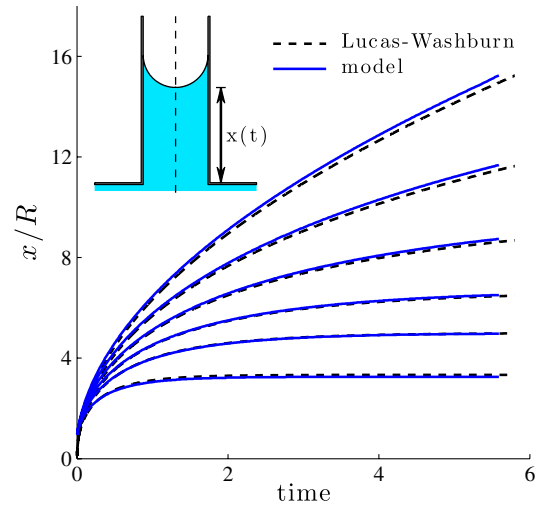


FIG. 5 (color online). Capillary rise experiments. We compare the model predictions with the Lucas-Washburn theory for different values of the Bond number $Bo = \{0, 0.1, 0.2, 0.3, 0.4, 0.6\}$. We set $\gamma \cos\theta/8\eta_w = 10$ and $\eta_w/\eta_g = 1000$.

angle is a fascinating feature of our model, which emanates from the competing effects of the various terms in the governing equations. Other interesting features of capillary phenomena in confined geometries could be analyzed with extensions of the proposed model. These may include instabilities in core-annular flow [32] or the effect of spatial variations in pore geometry and surface properties [11,33,34], limited to cases where the 1D upscaling is appropriate.

As a further quantitative assessment of the model predictions, we consider the rise of a meniscus in a vertical capillary, as predicted by our model and the Lucas-Washburn theory (Fig. 5). The dimensionless parameter comparing gravitational and capillary forces is the Bond number $Bo = \Delta\rho g R^2 / \gamma \cos\theta$, where $\Delta\rho = \rho_w - \rho_g$ is the density difference between fluids.

It is well understood that upscaling capillary phenomena often requires higher-order mathematical models. Surprisingly, it has been commonly accepted that upscaled descriptions of important multiphase flows, in particular, flow through porous media, can be cast as second-order, nonlinear advection-diffusion equations. Here we show that a phase-field formulation captures static and dynamic features of such flows that are precluded within the classical theories. Local, nonspreading structures, which are characteristic of partially wetting systems, can be obtained as steady-state solutions in the absence of external forces. Pseudodynamic effects emerge naturally as the transition from the capillary-dominated regime to the viscous-dominated regime. The present study suggests that a paradigm shift towards higher-order models in the macroscopic description of multiphase flow through porous media may henceforth be warranted [35].

Funding for this research was provided by Eni S.p.A. under the Multiscale Reservoir Science project and by the ARCO Chair in Energy Studies.

[1] M. Alava, M. Dubé, and M. Rost, *Adv. Phys.* **53**, 83 (2004).
 [2] D. I. Dimitrov, A. Milchev, and K. Binder, *Phys. Rev. Lett.* **99**, 054501 (2007).
 [3] C. W. MacMinn, M. L. Szulczewski, and R. Juanes, *J. Fluid Mech.* **662**, 329 (2010).
 [4] H. P. Greenspan, *J. Fluid Mech.* **84**, 125 (1978).
 [5] A. Oron, S. H. Davis, and S. G. Bankoff, *Rev. Mod. Phys.* **69**, 931 (1997).
 [6] G. I. Barenblatt, *Scaling, Self-Similarity and Intermediate Asymptotics* (Cambridge University Press, Cambridge, England, 1996).

[7] J. Bear, *Dynamics of Fluids in Porous Media* (Wiley, New York, 1972).
 [8] P. G. de Gennes, *Rev. Mod. Phys.* **57**, 827 (1985).
 [9] D. Bonn, J. Eggers, J. Indekeu, J. Meunier, and E. Rolley, *Rev. Mod. Phys.* **81**, 739 (2009).
 [10] R. L. Hoffman, *J. Colloid Interface Sci.* **50**, 228 (1975).
 [11] M. Queralt-Martín, M. Pradas, R. Rodríguez-Trujillo, M. Arundell, E. Corvera Poiré, and A. Hernández-Machado, *Phys. Rev. Lett.* **106**, 194501 (2011).
 [12] F. P. Bretherton, *J. Fluid Mech.* **10**, 166 (1961).
 [13] G. I. Taylor, *J. Fluid Mech.* **10**, 161 (1961).
 [14] A. de Lozar, A. L. Hazel, and A. Juel, *Phys. Rev. Lett.* **99**, 234501 (2007).
 [15] D. A. Weitz, J. P. Stokes, R. C. Ball, and A. P. Kushnick, *Phys. Rev. Lett.* **59**, 2967 (1987).
 [16] J. P. Stokes, A. P. Kushnick, and M. O. Robbins, *Phys. Rev. Lett.* **60**, 1386 (1988).
 [17] S. M. Hassanizadeh and W. G. Gray, *Water Resour. Res.* **29**, 3389 (1993).
 [18] K. T. Tallakstad, H. A. Knudsen, T. Ramstad, G. Løvoll, K. J. Måløy, R. Toussaint, and E. G. Flekkøy, *Phys. Rev. Lett.* **102**, 074502 (2009).
 [19] P. G. Saffman and G. I. Taylor, *Proc. R. Soc. A* **245**, 312 (1958).
 [20] J. P. Stokes, D. A. Weitz, J. P. Gollub, A. Dougherty, M. O. Robbins, P. M. Chaikin, and H. M. Lindsay, *Phys. Rev. Lett.* **57**, 1718 (1986).
 [21] G. Løvoll, M. Jankov, K. J. Måløy, R. Toussaint, J. Schmittbuhl, G. Schäfer, and Y. Méheust, *Transp. Porous Media* **86**, 305 (2011).
 [22] B. G. Cox, *J. Fluid Mech.* **14**, 81 (1962).
 [23] P. Aussillous and D. Quéré, *Phys. Fluids* **12**, 2367 (2000).
 [24] V. S. Ajaev and G. M. Homsy, *Annu. Rev. Fluid Mech.* **38**, 277 (2006).
 [25] P. G. de Gennes, *J. Chem. Phys.* **72**, 4756 (1980).
 [26] W. E and P. Palfy-Muhoray, *Phys. Rev. E* **55**, R3844 (1997).
 [27] J. W. Cahn and J. E. Hilliard, *J. Chem. Phys.* **28**, 258 (1958).
 [28] H.-G. Lee, J. S. Lowengrub, and J. Goodman, *Phys. Fluids* **14**, 492 (2002).
 [29] T. P. Witelski, *Appl. Math. Lett.* **11**, 127 (1998).
 [30] R. Benzi, M. Sbragaglia, M. Bernaschi, and S. Succi, *Phys. Rev. Lett.* **106**, 164501 (2011).
 [31] A. L. Bertozzi, A. Münch, X. Fanton, and A. M. Cazabat, *Phys. Rev. Lett.* **81**, 5169 (1998).
 [32] R. W. Aul and W. L. Olbricht, *J. Fluid Mech.* **215**, 585 (1990).
 [33] H. Kusumaatmaja, C. M. Pooley, S. Girardo, D. Pisignano, and J. M. Yeomans, *Phys. Rev. E* **77**, 067301 (2008).
 [34] M. Sbragaglia, R. Benzi, L. Biferale, S. Succi, and F. Toschi, *Phys. Rev. Lett.* **97**, 204503 (2006).
 [35] L. Cueto-Felgueroso and R. Juanes, *Phys. Rev. Lett.* **101**, 244504 (2008).